Proceedings of HT2003
ASME Summer Heat Transfer Conference
July 21-23, 2003, Las Vegas, Nevada, USA

HT2003-47190

ASSESSMENT OF THE THERMAL PERFORMANCE OF ALTERNATE FIRING SCHEMES IN OXYGEN-FIRED GLASS MELTING FURNACES

Kris L. Jorgensen
The Babcock & Wilcox Company
20 S. Van Buren Avenue
Barberton, OH 44203
Email: KLJorgensen@babcock.com

Satish Ramadhyani
132 Cecil Street, S.E.
Minneapolis, MN 55414
Email: s_ramadhyani@hotmail.com

Raymond Viskanta
School of Mechanical Engineering
Purdue University
West Lafayette, IN 47904
Email: viskanta@ecn.purdue.edu

ABSTRACT

Three firing schemes for an industrial oxygen-fired glass melting furnace were examined to determine the thermal performance and relative merits of each scheme. A comprehensive computer model was used to investigate the effects of each scheme on the combustion and heat transfer in the furnace. The three-dimensional computer model, suitable for predicting and analyzing fluid flow, combustion and heat transfer has been used to simulate the combustion space of the furnace. The turbulent flow field is obtained by solving the Favre averaged Navier-Stokes equations and using the k-ε model to calculate the turbulent shear stresses and close the equation set. The combustion model consists of a single step, irreversible, infinitely fast reaction. A mixture fraction is used to track the mixing of fuel and oxidant and thus reaction progress in this mixing limited model. An assumed shape PDF method is utilized to account for turbulent fluctuations. Radiative heat transfer in the combustion gases and between surfaces is modeled using the discrete ordinates method coupled with the weighted-sum-of-gray-gases model. The model furnace for all three firing schemes was the same size and shape, was charged from the rear end wall and was pulled from the front wall. The three schemes investigated were: 1) non-interlaced side-wall fired, 2) interlaced side-wall fired, and 3) end fired.

The results show that all three arrangements provide similar thermal performance and heat transfer characteristics. However, the flow field for the non-interlaced arrangement is very complex in the region where jets from opposing walls meet at the furnace center line. This type of jet interference can lead to unstable flow, particularly at the centerline of the furnace. Unstable flow conditions can affect the heat transfer characteristics of the furnace and make the furnace difficult to operate. Conversely, the interlaced and end-fired schemes do not exhibit the jet interference seen in the non-interlaced arrangement. While the results indicate that the thermal performance of all three arrangements were similar, the possibility of jet interference suggests that an interlaced or end-fired arrangement is preferable.

INTRODUCTION

For many decades glass melting furnaces have been fired with standard air that has been substantially preheated with the use of regenerators. Typically, to accomplish this, air is passed through a regenerator on one side or the end of the furnace to preheat it, while exhaust gasses pass through a separate regenerator on the opposite side or end of the furnace to extract excess heat. Each burner on the sidewall is matched with an exhaust port on the opposite wall. The gas flow is periodically reversed so that not only is the role of the two regenerators reversed but also air and exhaust ports. This cross-firing technique has the benefit of increasing the overall efficiency of the melting process. However, the resulting high temperatures

in glass melting furnaces results in a high production rate of NOx. This causes difficulties when attempting to control NOx emissions from these furnaces.

In an effort to reduce pollutant emissions, standard air has been replaced with pure oxygen, produced on site, as the oxidant for the fuel. By removing the nitrogen from the oxidant the largest source of nitrogen within the combustion space is eliminated. Since the flame temperatures in oxygen flames are considerably higher than preheated air flames, the need for regenerators has diminished, and they have not typically been used in order to reduce the capital investment (Figure 1). Without regenerators there is no need to cycle the furnace. In a cross-fired furnace this eliminates the need for multiple exhaust ports on one side wall and allows burners to be placed there. The furnace is then simultaneously fired from both sides. Similar changes to other standard designs are possible. Since this technology is relatively new, many different oxygen firing design variations are being investigated.

With the recent advent of oxygen firing, designers have to deal with several new issues. Gridley [1] outlines some of these issues and how they affect furnace design compared to standard air-fired furnaces. For example, since the gas conditions in an oxygen fired furnace are very different from those in an air fired furnace new materials have had to be employed for furnace construction to reduce wear and corrosion of the refractory. Without having to place bulky regenerators on the furnace, there is more flexibility in burner location and exhaust placement. In this paper, three general firing schemes are examined to study the effects of burner placement. Two of the three, cross-fired with interlaced jets and cross-fired with non-interlaced jets, involve burners being placed on both side walls and fired simultaneously while exhausted at the furnace's front wall. The third, end fired, is fired from the furnace's rear wall and exhausted at the front wall. The three different designs are shown in Figure 2.

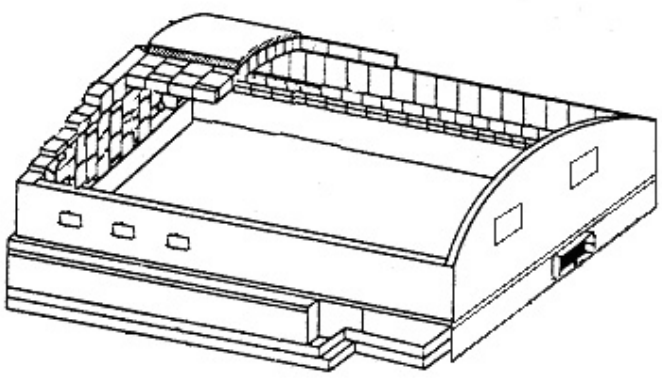

Figure 1. Representative oxygen-fired furnace with side-wall burners and front-wall exhaust.

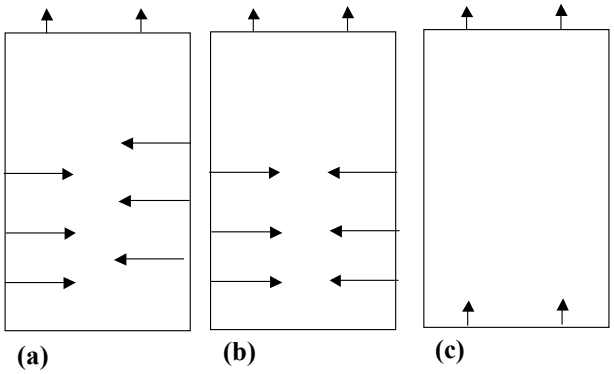

Figure 2. Schematic of three oxygen fired glass melting furnace designs: (a) interlaced-fired burners, (b) aligned-fired burners, and (c) end-fired.

MATHEMATICAL MODEL

Glass melting furnaces are characterized by a rectangular combustion space with a flat or arched roof. Walls and a roof that are insulated with refractory brick bound the combustion space. The glass load forms the floor. Modeling this type of system requires prediction of the mean flow field, turbulence, combustion reactions and heat transfer within the combustion space.

The thermal and fluid behavior is governed by a set of three-dimensional partial differential equations. This set includes the continuity equation, Navier-Stokes equations, and conservations of energy equation. The steady-state form of the governing equations is obtained using a density weight averaging also known as Favre averaging. The computational model involves the solution of this set of equations, the details of which have been given elsewhere [2].

Additional sub-models have been incorporated to increase its accuracy and usefulness. A brief description of the some of the sub-models is summarized here.

Turbulence Model

The averaging of the conservation equations introduces additional Reynolds stress terms that must be satisfied. These terms have been represented using the Boussinesq approximation. The eddy or turbulent viscosity is determined through the k-ε turbulence model [3, 4], where k is the turbulent kinetic energy and ε is the turbulent energy dissipation.

Combustion

Non-premixed combustion is modeled with a single step reaction that is mixing limited. The mixing rate is tracked through a conserved scalar, the mixture fraction, and turbulent effects are incorporated using an assumed clipped Gaussian PDF. This technique is detailed by Lockwood and Naguib [5] and presented by Kuo [6] for Favre averaged equations.

Radiation

The radiation transport within the combustion space of the furnace can be found from the solution of the radiative transfer equation. The discrete ordinates method (DOM), first used by Hyde and Truelove [7] and Truelove [8] for heat transfer, was selected due to its high accuracy and reasonable computational requirements. Spectral effects due to gas specie concentration are approximated through the weighted-sum-of-gray-gases model (WSGG).

Solution Method

The control volume method is used to obtain discretized versions of all the differential conservation equations [9]. The discretized equations are solved using an iterative technique, which traverses the computational domain in a line-by-line fashion. The SIMPLER algorithm [9, 10] is employed to treat the coupling between the continuity and momentum equations. The thicknesses of the walls and roof of the furnace were excluded from the computational domain, and the thermal boundary conditions were applied at the inside surfaces of the walls and roof as well as at the surface of the glass bath at the bottom of the furnace.

GLASS FURNACE DESCRIPTION

In order to compare the effects of the different firing schemes, a common size of furnace was chosen such that all of the firing schemes could reasonably be used in an actual furnace application. It was felt that furnaces that used a 'U' shaped firing scheme or other end firing scheme were restricted in how large they could be in practice, whereas side fired furnaces can be used in a wider range of sizes including much larger furnaces. The horseshoe fired furnace reported by Cassiano et al. [11] was selected as the nominal design size permitting direct comparisons of all configurations being investigated without being concerned about practicality.

The furnace consisted of a rectangular enclosure with dimensions of 8.5 m long from front wall to rear wall, 5.1 m wide, and 2.2 m high. The rear wall is where the furnace is "charged" with the raw material (batch). This end of the furnace is also referred to as the charge end. The molten glass is pulled from the furnace through a narrow throat in the front wall. This end of the furnace is also referred to as the throat end. The furnace had a thermal capacity of 5.75 MW and was fired with natural gas with 2.5% excess oxygen. Each of the arrangements investigated used this same size furnace and firing rate.

MODEL VALIDATION AND GRID RESOLUTION

The mathematical model was validated against experimental data from two laboratory scale furnaces. Comparisons of model predictions and data from the International Flame Research Foundation (IFRF) [12] and Institute of Gas Technology (IGT) [13] have been made. The results of this validation effort have been reported elsewhere [2].

Required grid resolution was determined by comparing load heat fluxes for grids with a varying number of control volumes for a single representative simulation. Total heat flux results within 2 percent were obtained for the two most refined grids. The courser of the two (131,000 control volumes) was selected over the finer (233,000 control volumes) in an effort to reduce computational effort. While changes in geometry resulted in slight variations in the total number of control volumes, the study was used as a guideline to determine the required resolution.

Table 1. Summary of furnace configuration and firing conditions for all oxygen fired furnace schemes.

	Interlaced	Non-interlaced	End
Number of Burners	6	6	2
Burner Location	side wall	side wall	rear wall
Oxygen Port Size (W x H) m	0.75 x 0.048	0.75 x 0.048	1.59 x 0.048
O_2 Temperature (K)	583	583	583
O_2 Velocity (m/s)	3.8	3.8	5.7
Number of Fuel Ports per Burner	1	1	3
Fuel Temperature (K)	383	383	383
Fuel Velocity (m/s)	14.1	14.1	14.1
Fuel Port Size (W x H) (m)	0.13 x 0.02	0.13 x 0.02	0.13 x 0.02

BURNER CONFIGURATION AND FIRING CONDITIONS

Burners used in the furnace models consisted of a rectangular oxygen port with one or three rectangular fuel ports distributed uniformly under the oxygen port. The size of the oxygen port, the number of fuel ports, and the mass flow rates were determined by the required operating power. The size and number of burners used for each of the models is given in Table 1. The fuel used for these simulations was natural gas with a heating value of 41.76 MJ/kg and was approximated by the following mass composition: 75.22% CH4, 9.19% C2H6, 1.71% C3H8, 11.03% N2, 0.32% CO2, and 2.54% C4H10, while 100.0% O2 was used as the oxidizer. Also given in Table 1 are the firing conditions for each of the firing schemes examined.

The glass load boundary was simulated by assuming a portion of the glass surface was covered with the raw batch, another portion was only partially covered with batch and the remaining surface was exposed molten glass. The batch was assumed to cover 100% of the surface for the first meter from

the rear wall where the furnace was charged. The partially covered region started one meter from the rear of the furnace to two-fifths of the distance from the rear wall to the front wall. The coverage started at 100% and decreased parabolicly to zero from the rear to the front end of this region. The temperature of the batch was assumed to be at the melting point of the glass (1300 K). A parabolic glass temperature was applied to the molten glass with a peak value of 1750 K two-thirds of the distance from the rear wall to the front wall. The effective temperature for control surfaces partially covered with batch was determined using an area-weighted combination of the batch temperature and glass temperature.

RESULTS AND DISCUSSION

Flow Patterns

Of primary interest of the new design is gas flow structure through the furnace. The intent of offsetting the burners on opposite walls was to allow the burner jets to penetrate past the center of the furnace to form an interlaced pattern. This arrangement has two advantages that the fuel and oxygen from each jet would be allowed to mix and burn without interference from other jets, while at the same time provide a evenly distributed heat flux to the load.

Figure 3 shows velocity vectors in a horizontal plane through the oxygen inlet port for the interlaced burner design. This plane is taken 0.6 m above the glass surface. The six inlet streams, three from each side wall, are evident in this figure. The inlet streams from each of the burners penetrate into the furnace and interlace near the furnace centerline as intended. Even though the burners on each side wall are staggered with respect to the opposite wall, the jets do not interlace with each other to a great extent. The jets from opposite walls clearly interfere with each other. All six jets are affected to some degree by the flow from other burners and the bulk flow through the furnace.

Some of the more significant jet interference is evident where the burner closest to the rear wall on the right-hand side and the center jet on the left-hand side impinges against each other in the middle of the furnace. Jets on the opposite wall divert both of these gas streams toward each other. The jet closest to the rear wall on the right-hand side wall is pushed toward the front wall by the flow from the rear most jet on the left-hand side wall. The middle jet on the right-hand side wall is able to penetrate a considerable distance into the furnace and force the middle jet on the left-hand side wall toward the rear of the furnace. Also notable, the jets closest to the front wall are turned toward the exhaust ports located on the front wall from the bulk flow of gases moving toward the exhaust ports.

Velocity vectors on a vertical plane through the center of the third burner shows how flow from the opposite wall affects the flow from this burner. The jet is not able to fully penetrate before it is turned upward by flow from the opposite wall.

The interlaced-fired arrangement of burners generates a very complex flow pattern within the furnace. As can be seen in Figures 3 and 4, several small recirculation patterns have developed. Many of them are caused by jets on opposite walls as they pass within close proximity to each other.

The non-interlaced-fired design is similar to the interlaced design except the jets are place directly opposite each other. This arrangement ignores the issues associated with opposing jets impinging on each other. Figure 5 shows the velocity vectors for the horizontal plane through the oxygen inlet ports for this geometry.

As expected each burner jet impinges against the burner jet from the opposite wall. Generally, the bulk flow from each burner is fairly simple, impinging on the opposite jet and then progressing to the outlets. However, the flow field between the

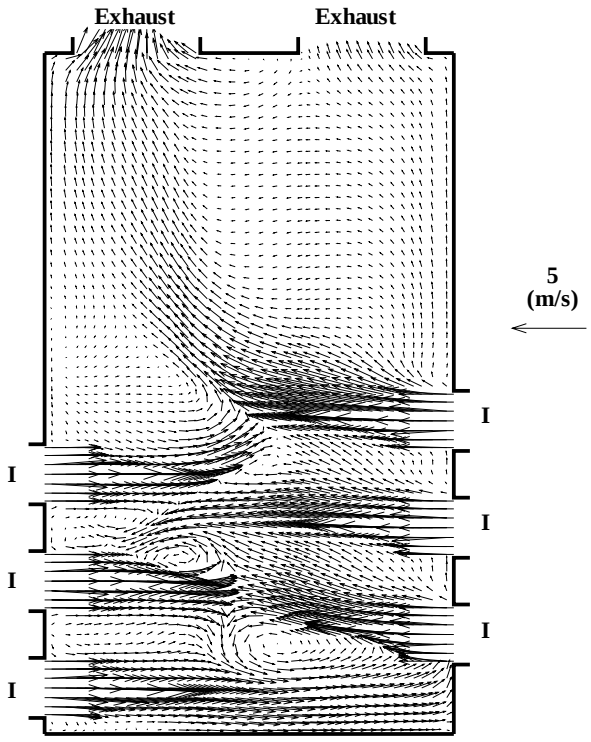

Figure 3. Velocity vectors for the horizontal plane through the oxygen inlet for the interlaced-fired design.

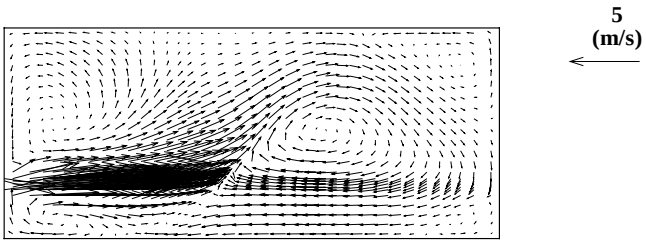

Figure 4. Velocity vectors for the vertical plane centered in the third burner from the rear end of the interlaced-fired design.

burner jets is very complex. Recirculation patterns that have developed interact with each other. This is most clearly seen between the first and second burner pairs from the rear wall.

Vectors on the vertical plane through the third and fourth burners (Figure 6) show how the gases are forced mostly upward where the two jets meet. This creates two large recirculation zones on each side of the furnace above the burner jets. This motion also carries hot combustion gases toward the roof of the furnace. Large recirculating patterns such as these can have a significant impact on the heat transfer characteristics of the furnace. Transporting large quantities of hot gasses to other parts of the furnace can increase heat loss to the walls and significantly alter the heat flux distribution to the load.

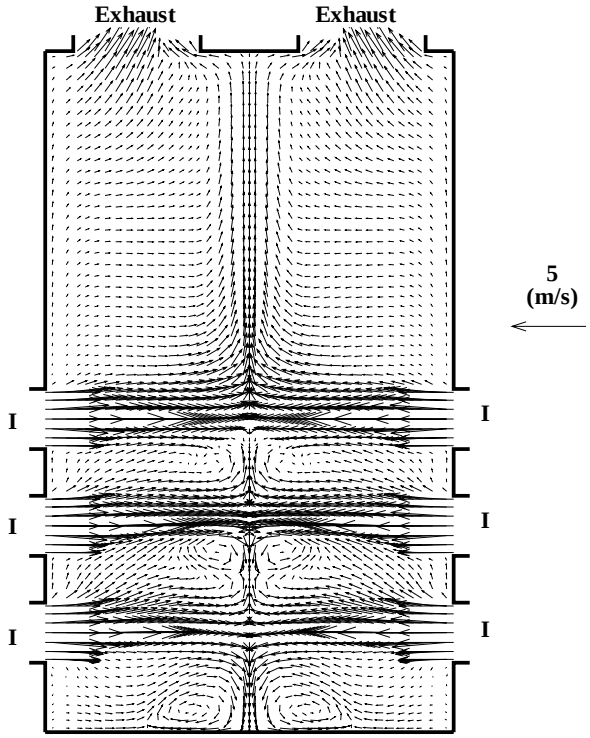

Figure 5. Velocity vectors for the horizontal plane through the oxygen inlet for the aligned-fired design.

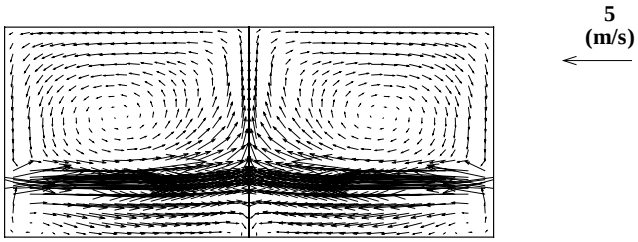

Figure 6. Velocity vectors for the vertical plane centered in the third and fourth burner from the rear end of the non-interlaced-fired design.

A separate concern that can't be addressed by a time-averaged simulation is the stability of the flow where the jets impinge on each other. It is possible that instead of impinging directly against each other, small perturbations in the flow will cause the jets to rapidly move from one side to the other. This type of instability is difficult to control and the effect is equally difficult to predict.

The third design that was examined was the end-fired arrangement. Instead of firing from the side walls, the burners are placed at one end of the furnace and exhausted at the other end. The flow field is presented in Figure 7 for a horizontal plane through the oxygen inlet ports. The flow field for the end-fired furnace is void of the large recirculation seen in the other arrangements for the plane. Since the inlet and the exhaust ports are aligned, the flow is essentially straight from the inlet to the exhaust.

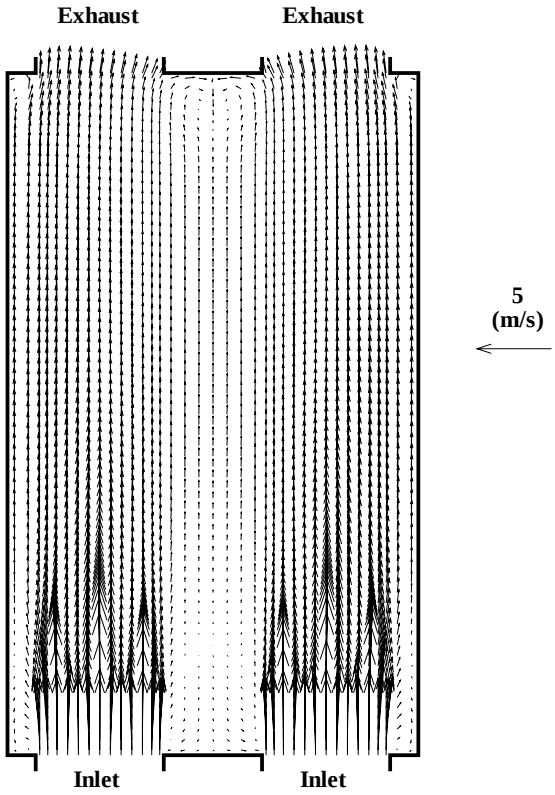

Figure 7. Velocity vectors for the horizontal plane through the oxygen inlet for the end-fired design.

Gas Temperature Profile

Gas temperatures on the horizontal plane through the burners for all three designs are compared in Figure 8. In all three designs temperatures are highest near the inlet ports where the fuel and oxygen are mixing and the heat of combustion is being released. Further into the furnace, the temperatures begin to decrease after the fuel has mixed with the

oxygen and burned. At each burner, distinct regions of high temperatures extend from the inlet port into the furnace. This is where the oxygen and the fuel are reacting on the outside edges of the fuel inlet stream. As the hot combustion gases pass through the furnace heat losses to the load continue to decrease the temperature.

For the two side wall fired arrangements it can be seen that the region of highest heat release is near the side walls and is before the individual jets interfere with each other. This is an important observation. As discussed, the flow patterns are very complex toward the center of the furnace for these tow designs. The concern is that opposing jets will interfere with proper and complete combustion. However, as can be seen in Figure 8, combustion is essentially complete before opposing jets meet.

The majority of the heat release for the two side wall fired arrangements is in the rear half of the furnace. In contrast, the majority of the heat release for the end-fired arrangement is the rear third of the furnace.

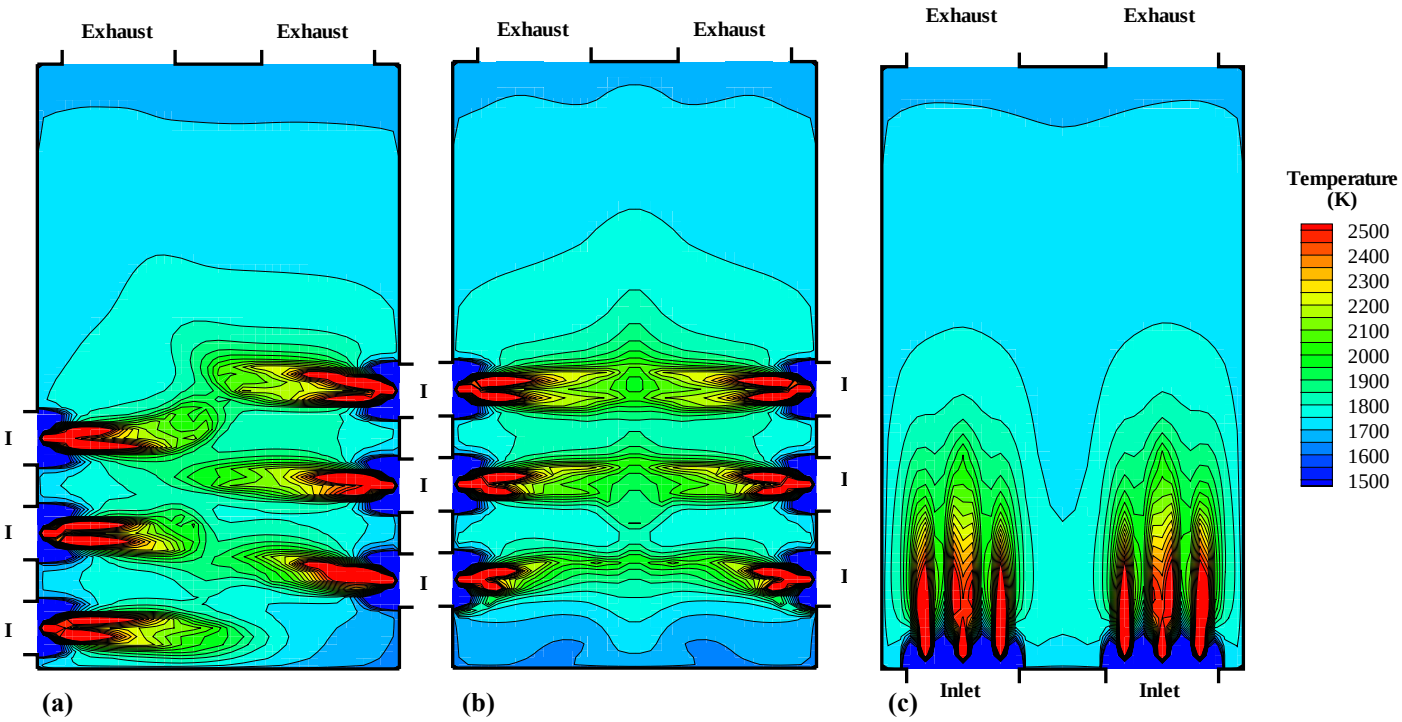

Figure 8. Comparison of iso-therms on a horizontal plane located 0.6 m above the glass surface for (a) interlaced-fired burners, (b) aligned-fired burners, and (c) end-fired.

Load Heat Flux Distribution

The glass load heat flux for all three designs is shown in Figure 9. The local heat fluxes for all three designs ranged from about 10 kW/m^2 to about 140 kW/m^2. The regions of peak heat flux are located under each of the burners and correspond to the location where the majority of the heat from combustion is released. The heat flux on the load surface is highest of the region covered with batch and decreases rapidly over the molten glass due to the higher surface temperature in that region.

The heat flux pattern follows the heat release pattern from the combustion space. The high heat flux region for the side wall fired arrangements is the read half of the furnace while that of the end-fired arrangement was in rear third of the furnace. In all three cases, high heat flux region corresponded to the batch coverage.

For these simulations, a batch coverage profile was specified. In the case were the shape may be significantly different than what was assumed, the differences in heat flux distribution could become significant.

CONCLUSIONS

Selected results for each case have been summarized in Table 2. The efficiency reported here represents the portion of the total energy input transferred to the glass load. The losses include all heat transfer to the surrounding walls through convection and radiation and radiative losses to the inlet and outlet. The exhaust temperature is the bulk temperature of the exhaust gases.

The results shown in Table 2 indicate that all three of the cases performed nearly identically with respect to thermal efficiency and heat transfer to the load. In fact, the differences observed for all model output parameters reported here are negligible.

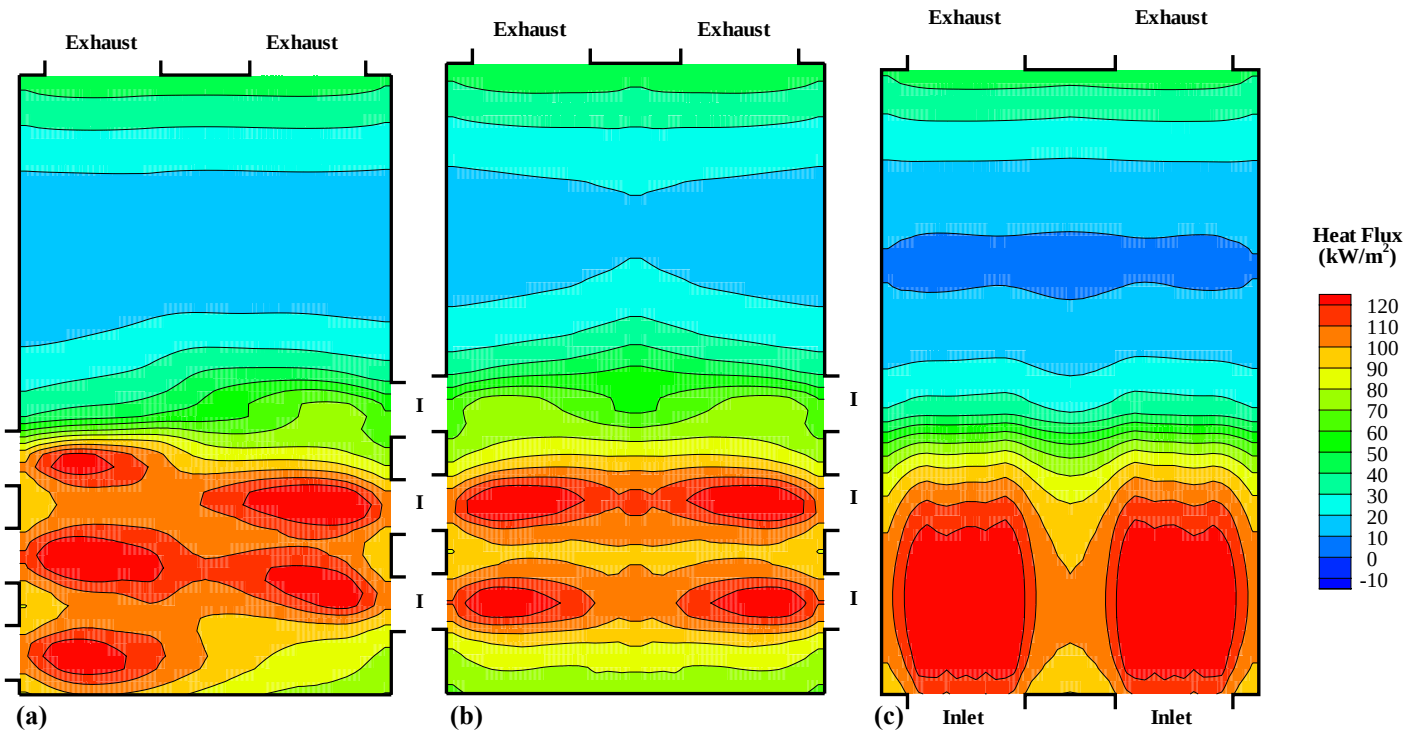

Figure 9. Comparison of load heat flux for (a) interlaced-fired burners, (b) aligned-fired burners, and (c) end-fired.

While the global values, reported in Table 2, show no significant difference, the flow patterns observed (Figures 3 -7) reveal that there are indeed significant differences. In particular, the flow field for the cross-firing was very complex and possibly unstable. In contrast, the flow field for the end fired design is uniform and stable.

For all three firing arrangements, sufficient time and space was available to complete combustion. For the two cross-fired arrangements, the combustion was mostly complete before the jets from opposite side walls reached the centerline. This is significant, particularly for the non-interlaced arrangement. Had the combustion zone extended to the centerline, where the flow field becomes unstable, it would be very difficult to predict how this would affect the flow field and heat transfer. For all three cases, the majority of the heat release from combustion coincided with the region over the batch material. This had the effect of improving heat transfer due to greater temperature difference between the gases and the batch/glass surface.

From these results the interlaced cross-fired and the end-fired designs are acceptable arrangements. The global results indicate that the non-interlaced arrangement produces similar results to the other arrangements; however, because of the complex flow patterns, possible burner jet interference and unstable flow, this design should be avoided.

Table 2. Comparison of selected results from simulations for all oxy-fired furnace schemes.

	Interlaced	Non-interlaced	End
Heat Absorbed by Load (MW)	2.98	2.97	2.95
Advected Out (MW)	1.49	1.49	1.48
Thermal Efficiency (%)	51.8	51.7	51.4
Average Load Heat Flux (kW/m^2)	68.6	68.5	68.1
Heat Flux Range (kW/m^2)	12.0-142.2	14.5-136.2	8.9-141.5

REFERENCES

[1] Gridley, M., 1996, "Philosophy, Design, and Performance of Oxy-Fuel Furnaces," In *57th Conference on Glass Problems*, Columbus, OH, American Ceramic Society.

[2] Jorgensen, K. L., 2001, *Three-dimensional Model for Assessing Fuel Distribution on Air and Oxygen Fired Glass Melting Furnace Performance*, Ph.D. Thesis, School of Mechanical Engineering, Purdue University, West Lafayette, IN.

[3] Jones, W. P. and Launder, B. E., 1972, "The Prediction of Laminarization with a Two-Equations Model of Turbulence," *International Journal of Heat and Mass Transfer*, 5, pp. 301–314.

[4] Launder, B. E. and Spalding, D. B., 1974, "The Numerical Computation of Turbulent Flows," *Computer Methods in Applied Mechanics and Engineering*, 3, pp. 269–289.

[5] Lockwood, F. C. and Naguib, A. S., 1975, "The Prediction of the Fluctuations in the Properties of Free, Round-Jet, Turbulent, Diffusion Flames," *Combustion and Flame*, 24, pp. 109–124.

[6] Kuo, K. K., 1986, *Principles of Combustion*, John Willey & Sons Inc, New York.

[7] Hyde, D. J. and Truelove, J. S., 1977, *The Discrete Ordinates Approximation for Multi-Dimensional Radiant Heat Transfer in Furnaces*, Technical Report AERE-R 8502, Heat Transfer and Fluid Flow Service, AERE Harwell, United Kingdom.

[8] Truelove, J. S., 1978, *Evaluation of a Multi-flux Model for Radiative Heat Transfer in Cylindrical Furnaces*, Technical Report AERE-R 9100, Heat Transfer and Fluid Flow Service, AERE Harwell, United Kingdom.

[9] Patankar, S. V., 1980, *Numerical Heat Transfer and Fluid Flow*, Hemisphere Publishing Corp., New York.

[10] Patankar, S. V., 1979, "A Calculation Procedure for Two-Dimensional Elliptic Situations," *Numerical Heat Transfer*, 2, pp 57-69.

[11] Cassiano, J., Heitor, M. V., and Silva, T. F., 1994, "Combustion Tests on an Industrial Glass-melting Furnace," *Fuel*, 73(10), pp. 1638–1642.

[12] Nakamura, T., Kamp, W. L. van de, and Smart, J. P., 1991, *Further Studies on High Temperature Natural Gas Combustion in Glass Furnaces*, Technical Report IFRF Doc. No. F 90/y/7 International Flame Research Foundation, Ilmjuiden, The Netherlands.

[13] Grosman, R. E. and Abbasi, H. A., 1996, *Combustion and Heat-Transfer Data Acquisition in a Glass Tank Simulator*, Technical Report GRI-96/0279 Gas Research Institute.